Novel β-amyloid PET Imaging Study of [^{18}F]92 in Patients with Cognitive Decline

Ming Ni,[¶] Xingxing Zhu,[¶] Kaixuan Wang, Wenliang Guo, Qin Shi, Yuying Li, Mengchao Cui,* and Qiang Xie*

ACCESS | 📊 Metrics & More | 📄 Article Recommendations

[^{18}F]92 Auto-radiochemical Synthesis   [^{18}F]92 Injection   [^{18}F]92 PET/CT images
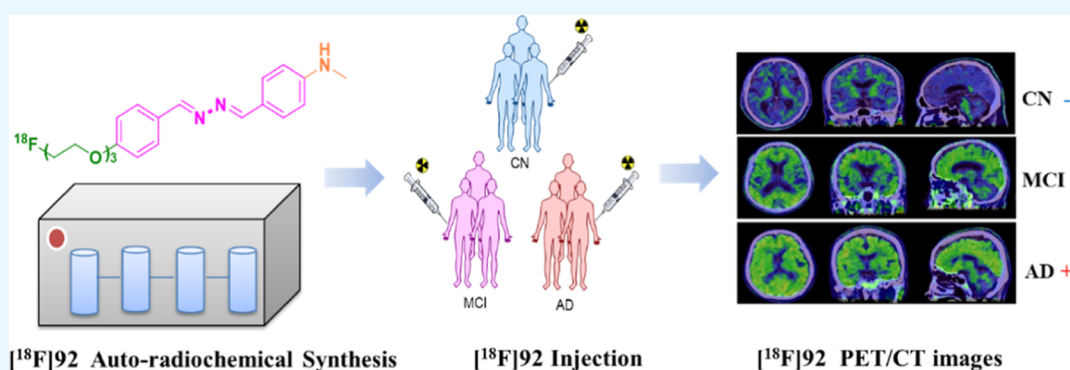
ABSTRACT: [^{18}F]-4-((E)-(((E)-4-(2-(2-(2-Fluoroethoxy)ethoxy)ethoxy)benzylidene)-hydrazono)methyl)-N-methylaniline ([^{18}F]92) is a novel positron emission tomography (PET) tracer previously reported to exhibit high binding affinity to aggregated β-amyloid (Aβ). This study aims to report a fully automated radiosynthesis procedure for [^{18}F]92, explore its radioactive distribution in the brains of healthy subjects, and investigate its potential application value in the early diagnosis of Alzheimer's disease (AD). The fully automated radiosynthesis of [^{18}F]92 was performed on the AllinOne module. Thirty one participants were recruited for this study. Dynamic [^{18}F]92 PET imaging was conducted over 0−90 min period to assess time−activity curves (TAC) and standardized uptake value ratio (SUVR) curves in cognitively normal (CN) subjects. All participants were visually classified as either positive (+) or negative (−). Semiquantitative analyses of [^{18}F]92 were performed by calculating SUVRs in different regions of interest. Furthermore, the study analyzed the relationships between global SUVR and plasma AD biomarkers, including Aβ_{42}, Aβ_{40}, P-tau181, and T-tau. The automated radiosynthesis of [^{18}F]92 was completed within 50 min, yielding a radiochemical purity of greater than 95% and a radiochemical yield of $36 \pm 3\%$ (nondecay-corrected). Among the participants, 15 were estimated as Aβ (−) and 16 as Aβ (+). TACs indicated that [^{18}F]92 rapidly crossed the blood−brain barrier within 10 min, followed by a rapid decrease, which then slowed down in the last 50−90 min. SUVR curves revealed that SUVR values stabilized around 60−70 min after injection and reached an equilibrium between 70 and 90 min, primarily in the cerebral cortex. SUVRs of Aβ (+) participants were significantly higher than those of Aβ (−) individuals within the cerebral cortex. In addition, Aβ_{42} and the Aβ_{42}/Aβ_{40} ratio exhibited negative correlations with global SUVR, while plasma P-tau181 and the P-tau181/T-tau ratio displayed positive correlations with global SUVR. [^{18}F]92 exhibits excellent pharmacokinetic properties in the human brain and can be synthesized automatically on a large scale. [^{18}F]92 is a promising and reliable radiotracer for estimating Aβ pathology accumulation, providing valuable assistance in AD diagnosis and guiding clinical trials of therapeutic drugs.

■ INTRODUCTION

Alzheimer's disease (AD) is a progressive neurodegenerative disorder that accounts for the majority of cases of senile dementia. It is characterized by the aggregation of extracellular β-amyloid (Aβ) plaques and the formation of intracellular neurofibrillary tangles (NFTs) composed of tau protein in cerebral tissue.[1,2] According to the Aβ cascade hypothesis, excessive Aβ deposition is an early event in AD, occurring before other pathophysiological processes such as NFTs, neuroinflammation, synaptic dysfunction, and neuronal death.[3−5]
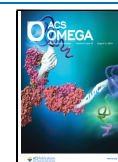
The Aβ deposition is believed to occur 10−30 years before the onset of dementia symptoms.[6] Therefore, the National Institute
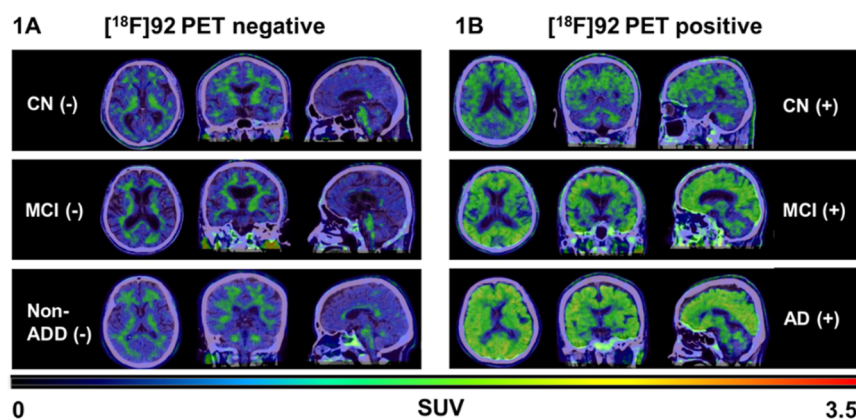
Figure 1. [18F]**92** PET/CT images in different diagnosed participants. (A) showed the group of [18F]**92** negative (1 CN: male, 72 y, MMSE = 27, CDR = 0; 1 MCI: male, 64 y, MMSE = 26, CDR = 0.5; 1 Non-ADD: female, 52 y, MMSE = 8, CDR = 1). (B) (1 CN: male, 69 y, MMSE = 28, CDR = 0; 1 MCI: male, 66 y, MMSE = 16, CDR = 0.5; 1 AD: female, 57 y, MMSE = 4, CDR = 1).

Table 1. Demographic and Clinical Characteristics of all Participants[a]

characteristic	total ($n = 31$)	$A\beta$ (−) ($n = 15$)	$A\beta$ (+) ($n = 16$)	test value	p value
gender, M/F	15/16	8/7	7/9	0.285	0.724
age, mean (SD), years	62.58(7.77)	60.00(8.87)	65.00(5.87)	−1.704	0.088
education, mean (SD), years	9.52(3.89)	9.40(3.92)	9.63(4.00)	−0.020	0.984
APOE $\varepsilon4$ carriers, n (%)	17(54.8%)	5(33.3%)	12(75.0%)	5.427	0.020
MMSE, mean (SD)	23.03(6.75)	22.73(8.73)	16.31(7.24)	−0.020	0.018
CDR, mean (SD)	0.65(0.57)	0.37(0.58)	0.91(0.42)	−3.086	0.002

[a]SD: standard deviation; APOE: Apolipoprotein E; MMSE: Mini-Mental State Examination; CDR: Clinical Dementia Rating.

on Aging-Alzheimer's Association (NIA-AA) has proposed the $A\beta$-tau-neurodegeneration classification framework, which defines the presence of $A\beta$ as a pathological change indicative of AD.[7]

Currently, the assessment of changes in $A\beta$ pathology in the brain relies on measuring the levels of $A\beta_{42}$ and the $A\beta_{42}/A\beta_{40}$ ratio in plasma or cerebrospinal fluid (CSF), as well as utilizing $A\beta$ positron emission tomography (PET). While plasma offers greater accessibility and allows for repeated sampling compared to CSF, the low levels of $A\beta$ peptide in plasma and limitations in detection sensitivity have led to inconsistent results.[8] CSF, although more accurate for evaluating $A\beta$ load in the brain, is hindered by the invasiveness of collection, limiting its widespread clinical application.[8,9] In contrast, $A\beta$ PET holds promise in providing valuable insights into the pathology underlying dementia. Its visualization and quantitative analysis contribute to enhancing clinical evaluation, individualized management, and clinical trials.[10−12] Consequently, significant efforts have been dedicated to exploring and developing specific $A\beta$ radiotracers for PET scans.

[11C]Pittsburgh compound B ([11C]PIB) was the pioneer in successfully serving as a selective $A\beta$ radiotracer for clinical diagnosis.[13] However, the short radioactive half-life of [11C] ($t_{1/2} = 20.4$ min) rendered it inconvenient for widespread use. Subsequently, radiotracers labeled with [18F] ($t_{1/2} = 109.8$ min) were developed, including [18F]Florbetapir,[14] [18F]-Flutemetamol,[15] and [18F]Florbetaben,[16] all of which received approval from the U.S. Food and Drug Administration (FDA) in 2012, 2013 and 2014, respectively. These compounds, derivatives of Thioflavin T and stilbene scaffold, have demonstrated high sensitivity and specificity in detecting $A\beta$ deposition and predicting progression, as confirmed by related reports.[17,18] Nevertheless, they have consistently exhibited an

issue with high nonspecific binding in white matter, potentially disrupting early diagnosis and sensitive detection.[19]

Recently, we reported a novel asymmetric diaryl-azine-based $A\beta$ PET tracer, [18F]-4-((E)-(((E)-4-(2-(2-(2-fluoroethoxy)-ethoxy)ethoxy)benzylidene)-hydrazono)methyl)-N-methylani-line ([18F]**92**), with exceptional binding affinity to synthetic $A\beta$ aggregates and $A\beta$ plaques in the AD brain.[20] Notably, [18F]**92** demonstrated superior brain pharmacokinetic properties in both rodents and nonhuman primates. Furthermore, the first-human PET study with a small sample size indicated that [18F]**92** exhibited low white matter uptake and effectively bound to $A\beta$ pathology, enabling the differentiation of AD patient from healthy control subject. These findings collectively suggest that [18F]**92** holds promise as a PET tracer for visualizing $A\beta$ pathology in AD patients. Consequently, this study aims to report the fully automated radiosynthetic procedure for [18F]**92** and further investigate its pharmacokinetic properties in the human brain, along with its diagnostic value for AD in a large sample of subjects.

■ RESULTS AND DISCUSSION

Automatic Synthesis and Quality Control of [18F]92. The final [18F]**92** solution, filtered through a sterile 0.22 μm filter, appears as a colorless and transparent liquid without any suspended particles. pH testing confirmed a stable pH range of 6−7 within 3 h. The radiochemical purity, assessed through analytical HPLC, was determined to exceed 95%. The formulated [18F]**92** was obtained with nondecay corrected radiochemical yields of 36 ± 3% ($n = 8$) in 50 min.

Visual Assessment and Participant Characteristics. Thirty-one participants successfully completed all examinations. In this study, [18F]**92** PET can visually evaluate cerebral $A\beta$ status in individuals with normal cognition and cognitive
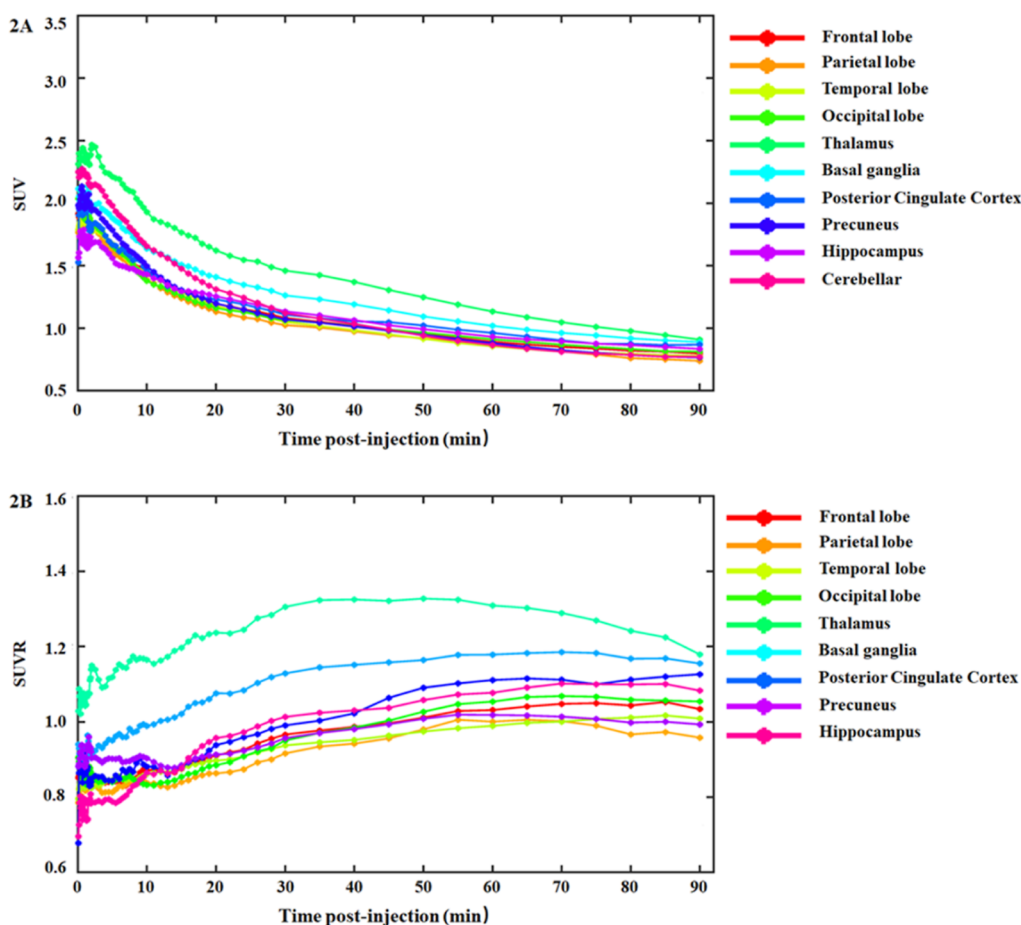
Figure 2. TACs (A) and SUVR curves (B) of $[^{18}F]$**92** PET in the same cognitive normal participant.

impairment. Among Aβ (−) individuals, $[^{18}F]$**92** retention was mainly restricted to white matter (Figure 1A), while Aβ (+) individuals showed $[^{18}F]$**92** deposition in the cerebral cortices (Figure 1B), as observed in various diagnosed cases. As a result, one participant in the cognitive normal (CN) group was identified Aβ (+), and six participants in the cognitive impairment (CI) group were Aβ (−). Therefore, 15 participants were ultimately categorized as Aβ (−), and 16 participants were designated as Aβ (+). The demographic and clinical characteristics of the two groups are presented in Table 1. No significant differences in gender, age, or education were observed between Aβ (−) and Aβ (+) groups. However, APOE ε4 carrier rate in the Aβ (+) group was significantly higher than that in the Aβ (−) group (p = 0.020). Additionally, neuropsychological tests, including MMSE and CDR, revealed poorer performance in the Aβ (+) group compared to the Aβ (−) group (p = 0.018, p = 0.002, respectively).

Time−Activity Curves of $[^{18}F]$92 PET in Cognitive Normal Participants. Two cognitively normal participants voluntarily underwent continuous dynamic PET acquisition for 90 min. TACs indicated that $[^{18}F]$**92** rapidly crossed the blood−brain barrier, peaking immediately after injection, and predominantly accumulated in the cortices within 10 min. Radioactivity exhibited a swift decline within the first 50 min postinjection, followed by a gradual decrease from 50 to 90 min (Figure 2A). SUVR curves revealed that SUVR values stabilized around 60−70 min after injection, reaching equilibrium between 70 and 90 min in most cortices (Figure 2B). In summary, our observations regarding the pharmacokinetic properties in

humans were consistent with our previous study in rhesus monkeys.[20] Consequently, all remaining participants underwent static $[^{18}F]$**92** PET acquisition from 60 to 90 min after injection.

Semi-quantitative Analyses of $[^{18}F]$92 PET. Semi-quantitative analyses (Table 2) indicated that the SUVRs in the $[^{18}F]$**92** positive group were significantly higher than those in the $[^{18}F]$**92** negative group in the major cerebral cortices including the bilateral frontal lobe, parietal lobe, temporal lobe, occipital gyrus, posterior cingulate cortex, precuneus, and deep gray matter-basal ganglia. However, no significant difference was observed in the bilateral hippocampus. In addition, the SUVR in the left thalamus was higher in the $[^{18}F]$**92** positive group compared to the $[^{18}F]$**92** negative group, but there was no significant difference in the right thalamus. Furthermore, a global SUVR of gray matter was calculated, showing higher accumulation in the $[^{18}F]$**92** positive group compared to the $[^{18}F]$**92** negative group (p < 0.001). The determined cutoff value for discriminating Aβ status was 1.18, with an AUC of 0.963.

Associations between $[^{18}F]$92 Uptake and Plasma AD Biomarkers. The plasma AD biomarkers of all participants were measured to further assess the associations with the global SUVR of $[^{18}F]$**92**. The results demonstrated that Aβ_{42} and the Aβ_{42}/Aβ_{40} ratio were negatively correlated with global SUVR (r = −0.616, p = 0.0002; r = −0.555, p = 0.001, respectively) (Figure 3A,C), while plasma P-tau181 and P-tau181/T-tau ratio exhibited a positive correlation with global SUVR (r = 0.515, p = 0.003; r = 0.568, p = 0.001, respectively) (Figure 3D,F). Besides, no significant associations were found between plasma Aβ_{40} and global SUVR (r = −0.024, p = 0.899) (Figure 3B), as well as

Table 2. Comparison With SUVR Between [18F]92 PET Negative and Positive

| parameter (SUVR)	normalized [18F]92 uptake		test value	p value
	Aβ (−)	Aβ (+)		
global gray matter	1.074 ± 0.040	1.367 ± 0.138	−8.144	<0.001
left cerebral area				
frontal lobe	1.088 ± 0.055	1.425 ± 0.160	−7.941	<0.001
parietal lobe	1.036 ± 0.076	1.373 ± 0.196	−6.392	<0.001
temporal lobe	1.050 ± 0.071	1.392 ± 0.150	−8.205	<0.001
occipital gyrus	1.185 ± 0.065	1.506 ± 0.206	−5.931	<0.001
thalamus	1.204 ± 0.095	1.284 ± 0.119	−2.062	0.048
basal ganglia	1.113 ± 0.091	1.285 ± 0.150	−3.832	<0.001
posterior cingulate cortex	1.225 ± 0.068	1.599 ± 0.172	−8.041	<0.001
precuneus	1.082 ± 0.072	1.543 ± 0.220	−7.926	<0.001
hippocampus	1.085 ± 0.095	1.094 ± 0.093	−0.258	0.799
right cerebral area				
frontal lobe	1.039 ± 0.060	1.363 ± 0.165	−7.358	<0.001
parietal lobe	0.954 ± 0.079	1.266 ± 0.185	−6.151	<0.001
temporal lobe	1.042 ± 0.044	1.356 ± 0.146	−8.218	<0.001
occipital gyrus	1.134 ± 0.065	1.462 ± 0.215	−5.813	<0.001
thalamus	1.272 ± 0.079	1.327 ± 0.112	−1.572	0.127
basal ganglia	1.172 ± 0.073	1.339 ± 0.140	−4.130	<0.001
posterior cingulate cortex	1.321 ± 0.082	1.541 ± 0.138	−5.456	<0.001
precuneus	1.139 ± 0.065	1.589 ± 0.218	−7.881	<0.001
hippocampus	1.123 ± 0.092	1.091 ± 0.107	−0.888	0.382

between T-tau and global SUVR ($r = 0.201$, $p = 0.286$) (Figure 3E).

This study marks the initial investigation of [18F]92 PET/CT in a diverse cohort of individuals with varying cognitive statuses, including cognitively normal subjects and those with cognitive impairments. This investigation revealed that [18F]92 efficiently crosses the blood−brain barrier, enters the brain within 3 min, and exhibits efficient clearance. The scans acquired at 60−90 min after injection provide stable SUVRs, so it can be recommended for static acquisitions. Previous research suggested the uptakes of the skull in reported Aβ or tau PET tracers were associated with off target, gender, and bone density, which may affect the quantitative analysis.[21] However, we observed no radioactive uptake of [18F]92 in the skull, as evidenced in both dynamic and static scans across all participants. These results align with previous research conducted in a nonhuman primate study,[20] which demonstrated that [18F]92 exhibits high binding affinity to Aβ aggregates (K_i = 10.1 ± 0.07 nM) and favorable lipophilicity (log D = 2.05 ± 0.07). Furthermore, the uptake pattern of [18F]92 in cerebral tissue closely resembles that of [18F]Florbetapir and [18F]-Florbetaben.[22,23] Due to its favorable brain pharmacokinetic properties, [18F]92 holds promise as a valuable tool for visualizing Aβ pathology by PET scans in AD.

Following standard practice, this study employed a classical binary classification for visually assessing brain Aβ status. The classification divided global Aβ pathology into two categories: positive and negative. Similar to the behavior of other clinically used Aβ PET radiotracers,[12,22] [18F]92 negative cases displayed restricted radiotracer binding primarily in the white matter, preserving the gray-white matter contrast. In contrast, [18F]92 positive cases exhibited cortical gray matter uptake equal to or greater than that in the white matter, leading to a loss of gray-white matter contrast. Meanwhile, the subjects with Aβ deposits showed more severe cognitive deterioration. Aβ PET is a crucial tool for diagnosing AD, but it is important to note that Aβ deposition also occurs in cognitively normal populations. Previous studies have indicated that the negative rate of Aβ PET falls within the range of 70 to 90% in cognitively normal older individuals. This means that a considerable percentage of them carry a significant Aβ burden, which is supposed to be related to the age and the presence of APOE ε4 allele,[24,25] potentially elevating their risk of developing MCI or dementia in subsequent years.[26] In our study, we observed mild [18F]92 retentions in the bilateral frontal lobe, parietal lobe, and temporal lobe of a 69 year-old CN subject carrying the APOE ε4
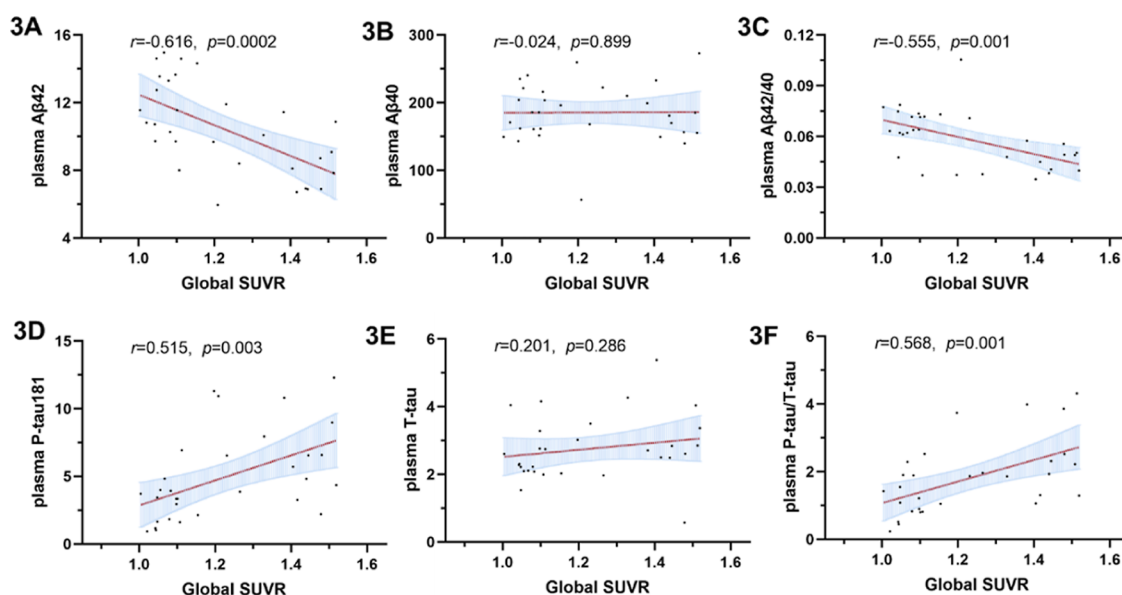
Figure 3. Associations between plasma AD biomarkers and global SUVR of [18F]92. (A−F): the associations between Aβ$_{42}$, Aβ$_{40}$, Aβ$_{42}$/Aβ$_{40}$ ratio, P-tau181, T-tau, P-tau181/T-tau ratio and global SUVR.

allele (Figure 3B). Consequently, we have been continuously monitoring the plasma AD biomarkers of this specific subject.

In this study, we employed the most widely accepted method to quantify the uptake of [18F]92 in regions known to exhibit Aβ deposition. We calculated the SUVRs of bilateral large regions of the cerebral cortex and deep gray matter, using the cerebellar gray matter as a reference. The results indicated that SUVRs of major gray matter regions in the Aβ+ group were significantly higher than those in the Aβ− group, consistent with our visual observations. However, the SUVRs of the bilateral hippocampus showed no significant difference between the left and right sides. This suggests that the hippocampus may lack sensitivity in discriminating Aβ status, possibly due to its relatively small volume and frequent association with cerebral atrophy, leading to partial volume effects.[27] Additionally, no significant difference in SUVR was observed in the right thalamus between the two groups, which is likely attributed to the limited sample size.

Global SUVR is a standard and valuable parameter for assessing the degree of global Aβ accumulation, increasingly used in antiamyloid clinical trials and for staging an individual's Aβ pathology progression.[28−33] In our study, global SUVR effectively distinguished the Aβ+ group from the Aβ− group with an impressive AUC of 0.963 at an SUVR threshold of 1.18. This cutoff value closely approximated the global SUVR thresholds reported in previous [18F]Florbetapir PET/CT studies, despite minor differences in data collection methods and reference brain regions.[34−37] Furthermore, we conducted an analysis of the correlations between plasma AD biomarkers and the global SUVR of [18F]92 to assess the consistency of cerebral Aβ deposition with plasma biomarkers. The results showed that Aβ42 and the Aβ42/Aβ40 ratio exhibited a negative correlation with global SUVR, while P-tau181 and the P-tau181/T-tau ratio displayed a positive correlation with global SUVR. These findings align with our previous research on the relationships between global SUVR from [18F]Florbetapir PET and plasma AD biomarkers in a cohort study on dementia population.[38] Currently, it is reported that commercially available Aβ PET were correlated with plasma AD biomarkers, and Aβ42/40 and P-tau181 demonstrated higher agreement with PET findings.[39−42] Therefore, the results of our study also validate the reliability of [18F]92 from this perspective. In addition, quantitative analysis of [18F]92 PET provides valuable insights for clinical applications.

This study has several limitations. First, the relatively small number of participants prevented an analysis based on MCI or dementia types. As a result, we are unable to discern the differences in Aβ deposition between MCI and AD patients as assessed by [18F]92 PET. Initial Aβ deposition is believed to occur in both the striatum and precuneus,[43] and Aβ deposition levels are weakly related to the severity of dementia symptoms in individuals with late-onset AD.[44] Therefore, a more comprehensive evaluation of the relationship between the degree of Aβ deposition and the AD continuum will be essential to confirm the clinical utility of [18F]92. This will be a focus of our future work, which will include a larger participant pool. Second, our study did not include dynamic scans for subjects with cognitive impairment, as they may have difficulty cooperating with longer examinations. Notably, previous studies have suggested that the washout speed of Aβ PET tracers in the cerebral cortex of AD patients is slower than that in normal controls.[45] Third, CSF AD biomarkers are complementary to Aβ PET and play a crucial role in clinical diagnosis and trials. However, this study did not assess the correlations between [18F]92 PET and CSF AD biomarkers.

CONCLUSION

In summary, [18F]92 could be synthesized automatically on a large scale using the AllinOne radiosynthesis module. It was prepared with a nondecay corrected radiochemical yield of 36 ± 3% and exhibited high radiochemical purity in less than 60 min. Dynamic PET scans of [18F]92 demonstrated excellent pharmacokinetic properties in the human brain, recommending static PET scans with imaging windows around 60−90 min. Both visual assessment and semiquantitative analyses indicate that [18F]92 is a promising novel radiotracer for estimating the location and extent of Aβ pathology accumulation, which is valuable for diagnosing AD and guiding clinical trials. Although [18F]92 PET exhibits some correlation with plasma AD biomarkers, further research with larger cohorts is needed to fully validate the clinical application of this tracer.

MATERIALS AND METHODS

Participants and Cognitive Assessments. A total of 38 initial participants, aged from 48 to 74, were recruited from the cognitive impairment center of the Department of Neurology at the First Affiliated Hospital of University of Science and Technology of China (USTC) between September 2020 and February 2021. Our study protocol was approved by the hospital ethics committee (2020KY-203) and conducted in accordance with the 1964 Declaration of Helsinki. Written informed consent for imaging was obtained from all participants. Comprehensive assessments were conducted, including detailed medical history collections, nervous system examination, brain magnetic resonance imaging (MRI) scan, and neuropsychological evaluation, including Mini-Mental State Examination (MMSE) and Clinical Dementia Rating (CDR) test. According to the NINCDS/ADRDA (National Institute of Neurological Disorders and Stroke−Alzheimer Disease and Related Disorders), DSM-IV (Diagnostic and Statistical Manual of Mental Disorders), and the revised consensus criteria of the International Working Group on Mild Cognitive Impairment (MCI),[46−49] participants were categorized into two groups: the cognitive normal (CN) group and the cognitive impairment (CI) group. The CN group had a CDR of 0, while the CI group had a CDR of 0.5 or greater. During the study, five participants from both the CN and CI groups withdrew, and three participants in the CI group were excluded due to scanning failure. The study flowchart is presented in Figure 4.

Chemicals and Reagents. The reagents and solvents were purchased from Sigma (Sigma-Aldrich, MO, USA) without further purification. The cartridges were purchased from Waters (Waters, MA, USA). The precursor of [18F]92 was obtained from Beijing Normal University.

Automatic Synthesis and Quality Control of [18F]92. For the automatic synthesis of [18F]92, the AllinOne module (Trasis, Ans, Belgium) was adapted and utilized at the Department of Nuclear Medicine, First Affiliated Hospital of USTC. [18F]Fluoride was produced on-site using the Eclipse RD Cyclotron system (Siemens Healthcare, Germany) by irradiating [18O]H2O with 11 MeV protons. The resulting [18F]fluoride was delivered to the radiosynthesis module and passed through a preactivated QMA cartridge. The trapped [18F]fluoride was eluted within a 1 mL solution of $K_{2.2.2}$/K_2CO_3 in acetonitrile− water (15 mg $K_{2.2.2}$ and 1.5 mg K_2CO_3, acetonitrile/water = 9:1, v/v). The mixture was then dried under vacuum conditions. Subsequently, 3.0 mg of precursor in 1.0 mL of anhydrous acetonitrile was added into the dried reactor, and the mixture
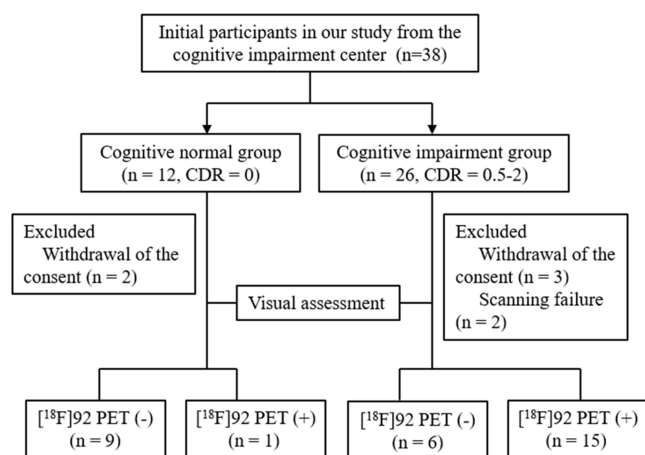
Figure 4. Flowchart shows the initial and excluded participant populations in this study.

was heated to 100 °C for 8 min. After cooling to room temperature, the reaction mixture was diluted with 7 mL of water and transferred to the HPLC loop under N_2 pressure. It was then injected into a semipreparative column and eluted with 60:40 CH_3CN/H_2O solution containing 500 mg NaAsc at a 5.0 mL/min flow rate. The formulated $[^{18}F]$**92** was captured in a C18 cartridge to remove the HPLC solvent and then formulated with EtOH and WFI (water for injection). The radiochemical purity was determined by analytical HPLC (Brownlee Validated AQ C18 Column −5 μm, 250 mm × 4.6 mm, Agilent Technologies, USA) using a 60:40 CH_3CN/H_2O mixture at a flow rate of 1.0 mL/min, monitored at $\lambda = 250$ nm.

$[^{18}F]$92 PET/CT Image Processing. $[^{18}F]$**92** PET/CT images were acquired from all participants using a PET/computed tomography (CT) scanner (Biograph 16HR, Siemens Healthcare, USA) at the Department of Nuclear Medicine, First Affiliated Hospital of USTC. Two CN subjects underwent dynamic brain scans immediately after tracer injection over a 0−90 min period, while the rest of the participants underwent PET scans within 60−90 min after injection. The administered dose of $[^{18}F]$**92** was measured at 259.0 ± 25.9 MBq. The time interval between body fluid detection and imaging examinations, including PET/CT and MRI scans, was maintained within three months for each participant. PET images were subsequently categorized as positive (+) or negative (−) through consensus reached by two professional physicians from the Department of Nuclear Medicine, following a binary visual assessment, as previously reported.[50]

PET Image Preprocessing and Analysis. Data preprocessing was carried out using SPM12 software (http://www.fil.ion.ucl.ac.uk/spm). Initially, the MRI T1W images were segmented into brain tissues and then spatially normalized to a custom template generated using DARTEL (Diffeomorphic Anatomical Registration Through Exponentiated Lie Algebra) methods. The frames of the whole uptake PET images were aligned to the middle frame. The middle frame was then coregistered to the corresponding T1 image and subsequently spatially normalized to the custom template. The spatial normalization transformation parameters were applied to the dynamic PET frames. Finally, all dynamic PET images were transformed into the montreal neurological institute (MNI) space and smoothed using a 6 mm full-width at half-maximum (fwhm) Gaussian kernel. This preprocessing was conducted for subsequent TAC analysis and SUVR analysis.

For ROI definition, the automated anatomic labeling (AAL) atlas was used. Atlas-based parcellation of PET images was employed to extract ROI encompassing the cerebellar regions, frontal lobe, parietal lobe, temporal lobe, occipital gyrus, thalamus, basal ganglia, posterior cingulate cortex, precuneus, and hippocampus. Gray matter probability map threshold at 0.8 was used as a global gray matter mask to derive the global SUVR. The standardized uptake value (SUV), calculated by normalizing mean ROI uptake using injected dose and body weight, was used to generate TAC for each dynamic PET frame. The cerebellar regions, positioned over cerebellar gray matter, were selected as the primary reference region for calculating SUVR.

Blood AD Biomarker Processing and Measurements. Plasma levels of $A\beta_{42}$, $A\beta_{40}$, P-tau181, and T-tau for all participants were assessed using the Simoa platform. Samples were collected and stored at −80 °C, then analyzed following the manufacturer's protocol. P-Tau181 was quantified using the P-tau181 Advantage V2 kit (Quanterix, 103714), while T-tau, $A\beta_{40}$, and $A\beta_{42}$ were measured using Neuro 3-plex A kit (Quanterix, 101195) on the HD-X platforms (Quanterix), following the manufacturer's instructions. Using PCR amplification and *Hha*I (NEB, R0139S) digestion to determine the Apolipoprotein E (APOE) genotype according to the previous study.[51] All samples were manually diluted and analyzed in duplicate.

Statistical Analysis. GraphPad Prism (Version 9.0; GraphPad Software, San Diego, CA) and SPSS software (Version 26.0; IBM Corp, Armonk, NY) were employed for all statistical analyses and chart creation. Categorical data were presented in frequency and percentage and analyzed by Pearson's chi-square test. For normally distributed continuous data, mean ± standard deviation and one-way analysis of variance were employed. Outliers, defined as data values exceeding three times the standard deviation of the mean, were excluded. The relationship between two variables was assessed using Pearson's correlation test if both data sets followed a normal distribution; otherwise, Spearman's rank test was adopted. The area under the ROC curves (AUC) served as a metric to quantify classifier performance. The cutoff value derived using maximizing Youden Index were adopted for differentiating $A\beta$ status. Two-tailed p-values less than 0.05 were considered indicative of statistical significance.

■ ASSOCIATED CONTENT

Data Availability Statement

The authors declare that the data in this article is available. This study was performed in line with the principles of the Declaration of Helsinki. Approval was granted by the Ethics Committee of the First Affiliated Hospital of University of Science and Technology of China (2020KY-203).

■ AUTHOR INFORMATION

Corresponding Authors

Mengchao Cui − *Key Laboratory of Radiopharmaceuticals, Ministry of Education, College of Chemistry, Beijing Normal University, Beijing 100875, China; Center for Advanced Materials Research, Beijing Normal University at Zhuhai, Zhuhai 519087, China;* ● orcid.org/0000-0002-3488-7864; Email: cmc@bnu.edu.cn

Qiang Xie − *Department of Nuclear Medicine, the First Affiliated Hospital of USTC, Division of Life Sciences and Medicine, University of Science and Technology of China, Hefei, Anhui 230001, China; School of Pharmacy, Bengbu*

Medical University, Bengbu 233000, China; Anhui Provincial Key Laboratory of Precision Pharmaceutical Preparations and Clinical Pharmacy, Hefei, Anhui 230001, China;
⊙ orcid.org/0000-0002-0974-1927; Email: xieqiang1980@ustc.edu.cn

Authors

Ming Ni − *Department of Nuclear Medicine, the First Affiliated Hospital of USTC, Division of Life Sciences and Medicine, University of Science and Technology of China, Hefei, Anhui 230001, China*

Xingxing Zhu − *Department of Nuclear Medicine, the First Affiliated Hospital of USTC, Division of Life Sciences and Medicine, University of Science and Technology of China, Hefei, Anhui 230001, China*

Kaixuan Wang − *Department of Nuclear Medicine, the First Affiliated Hospital of USTC, Division of Life Sciences and Medicine, University of Science and Technology of China, Hefei, Anhui 230001, China; School of Pharmacy, Bengbu Medical University, Bengbu 233000, China*

Wenliang Guo − *Department of Neurology, the Second Hospital of Anhui Medical University, Hefei, Anhui 230001, China*

Qin Shi − *Department of Nuclear Medicine, the First Affiliated Hospital of USTC, Division of Life Sciences and Medicine, University of Science and Technology of China, Hefei, Anhui 230001, China*

Yuying Li − *Key Laboratory of Radiopharmaceuticals, Ministry of Education, College of Chemistry, Beijing Normal University, Beijing 100875, China; Center for Advanced Materials Research, Beijing Normal University at Zhuhai, Zhuhai 519087, China*

Complete contact information is available at:
https://pubs.acs.org/10.1021/acsomega.4c03412

Author Contributions

¶M.N. and X.-X.Z. contributed equally to this work. M.-C.C. and Q.X. designed the study. W.-L. G., Q.S., Y.-Y.L. analyzed and organized the data. M.N. and X.-X.Z. performed the experiments. M.N. and Q.X. prepared the manuscript. X.-X.Z. and K.-X.W. synthesized and characterized the probes. All authors have given approval to the final version of the manuscript.

Notes

The authors declare no competing financial interest.
Consent to publish has been received from all patients included in this analysis. All patients signed a consent form.

■ **REFERENCES**

(1) Scheltens, P.; De Strooper, B.; Kivipelto, M.; Holstege, H.; Chételat, G.; Teunissen, C. E.; Cummings, J.; van der Flier, W. M. Alzheimer's disease. *Lancet* **2021**, *397*, 1577−1590.
(2) Moscoso, A.; Grothe, M. J.; Ashton, N. J.; Karikari, T. K.; Rodriguez, J. L.; Snellman, A.; Suárez-Calvet, M.; Zetterberg, H.; Blennow, K.; Schöll, M. Time course of phosphorylated-tau181 in blood across the Alzheimer's disease spectrum. *Brain* **2021**, *144*, 325−339.
(3) Jack, C. R.; Knopman, D. S.; Jagust, W. J.; Petersen, R. C.; Weiner, M. W.; Aisen, P. S.; Shaw, L. M.; Vemuri, P.; Wiste, H. J.; Weigand, S. D.; et al. Tracking pathophysiological processes in Alzheimer's disease: an updated hypothetical model of dynamic biomarkers. *Lancet Neurol.* **2013**, *12*, 207−216.
(4) McGeer, P. L.; McGeer, E. G. The amyloid cascade-inflammatory hypothesis of Alzheimer disease: implications for therapy. *Acta Neuropathol.* **2013**, *126*, 479−497.
(5) Wang, J.; Jin, C.; Zhou, J.; Zhou, R.; Tian, M.; Lee, H. J.; Zhang, H. PET molecular imaging for pathophysiological visualization in Alzheimer's disease. *Eur. J. Nucl. Med. Mol. Imaging* **2023**, *50*, 765−783.
(6) Hansson, O. Biomarkers for neurodegenerative diseases. *Nat. Med.* **2021**, *27*, 954−963.
(7) Jack, C. R.; Bennett, D. A.; Blennow, K.; Carrillo, M. C.; Dunn, B.; Haeberlein, S. B.; Holtzman, D. M.; Jagust, W.; Jessen, F.; Karlawish, J.; et al. NIA-AA Research Framework: Toward a biological definition of Alzheimer's disease. *Alzheimer's Dementia* **2018**, *14*, 535−562.
(8) Villa, C.; Lavitrano, M.; Salvatore, E.; Combi, R. Molecular and Imaging Biomarkers in Alzheimer's Disease: A Focus on Recent Insights. *J. Pers. Med.* **2020**, *10*, 61.
(9) Blennow, K.; Hampel, H. CSF markers for incipient Alzheimer's disease. *Lancet Neurol.* **2003**, *2*, 605−613.
(10) Shi, Z.; Fu, L. P.; Zhang, N.; Zhao, X.; Liu, S.; Zuo, C.; Cai, L.; Wang, Y.; Gao, S.; Ai, L.; et al. Amyloid PET in Dementia Syndromes: A Chinese Multicenter Study. *J. Nucl. Med.* **2020**, *61*, 1814−1819.
(11) Cotta Ramusino, M.; Perini, G.; Altomare, D.; Barbarino, P.; Weidner, W.; Salvini Porro, G.; Barkhof, F.; Rabinovici, G. D.; van der Flier, W. M.; Frisoni, G. B.; et al. Outcomes of clinical utility in amyloid-PET studies: state of art and future perspectives. *Eur. J. Nucl. Med. Mol. Imaging* **2021**, *48*, 2157−2168.
(12) Chapleau, M.; Iaccarino, L.; Soleimani-Meigooni, D.; Rabinovici, G. D. The Role of Amyloid PET in Imaging Neurodegenerative Disorders: A Review. *J. Nucl. Med.* **2022**, *63*, 13S−19S.
(13) Klunk, W. E.; Wang, Y.; Huang, G. F.; Debnath, M. L.; Holt, D. P.; Mathis, C. A. Uncharged thioflavin-T derivatives bind to amyloid-beta protein with high affinity and readily enter the brain. *Life Sci.* **2001**, *69*, 1471−1484.
(14) Choi, S. R.; Golding, G.; Zhuang, Z.; Zhang, W.; Lim, N.; Hefti, F.; Benedum, T. E.; Kilbourn, M. R.; Skovronsky, D.; Kung, H. F. Preclinical Properties of 18F-AV-45: A PET Agent for Aβ Plaques in the Brain. *J. Nucl. Med.* **2009**, *50*, 1887−1894.
(15) Nelissen, N.; Van Laere, K.; Thurfjell, L.; Owenius, R.; Vandenbulcke, M.; Koole, M.; Bormans, G.; Brooks, D. J.; Vandenberghe, R. Phase 1 Study of the Pittsburgh Compound B Derivative 18F-Flutemetamol in Healthy Volunteers and Patients with Probable Alzheimer Disease. *J. Nucl. Med.* **2009**, *50*, 1251−1259.
(16) Rowe, C. C.; Ackerman, U.; Browne, W.; Mulligan, R.; Pike, K. L.; O'Keefe, G.; Tochon-Danguy, H.; Chan, G.; Berlangieri, S. U.; Jones, G.; et al. Imaging of amyloid β in Alzheimer's disease with 18F-BAY94-9172, a novel PET tracer: proof of mechanism. *Lancet Neurol.* **2008**, *7*, 129−135.
(17) Villemagne, V. L. Amyloid imaging: Past, present and future perspectives. *Ageing Res. Rev.* **2016**, *30*, 95−106.
(18) Morris, E.; Chalkidou, A.; Hammers, A.; Peacock, J.; Summers, J.; Keevil, S. Diagnostic accuracy of (18)F amyloid PET tracers for the diagnosis of Alzheimer's disease: a systematic review and meta-analysis. *Eur. J. Nucl. Med. Mol. Imaging* **2016**, *43*, 374−385.
(19) Mountz, J. M.; Laymon, C. M.; Cohen, A. D.; Zhang, Z.; Price, J. C.; Boudhar, S.; McDade, E.; Aizenstein, H. J.; Klunk, W. E.; Mathis, C. A. Comparison of qualitative and quantitative imaging characteristics of [11C]PiB and [18F]flutemetamol in normal control and Alzheimer's subjects. *Neuroimage Clin.* **2015**, *9*, 592−598.
(20) Li, Y.; Zhou, K.; Zhang, X.; Zhao, H.; Wang, X.; Dong, R.; Wang, Y.; Chen, B.; Yan, X. x.; Dai, J.; et al. Fluorine-18-Labeled Diaryl-azines as Improved β-Amyloid Imaging Tracers: From Bench to First-in-Human Studies. *J. Med. Chem.* **2023**, *66*, 4603−4616.

(21) Flores, S.; Chen, C. D.; Su, Y.; Dincer, A.; Keefe, S. J.; McKay, N. S.; Paulick, A. M.; Perez-Carrillo, G. G.; Wang, L.; Hornbeck, R. C.; et al. Investigating Tau and Amyloid Tracer Skull Binding in Studies of Alzheimer Disease. *J. Nucl. Med.* **2023**, *64*, 287–293.

(22) Lundeen, T. F.; Seibyl, J. P.; Covington, M. F.; Eshghi, N.; Kuo, P. H. Signs and Artifacts in Amyloid PET. *Radiographics* **2018**, *38*, 2123–2133.

(23) Barthel, H.; Gertz, H. J.; Dresel, S.; Peters, O.; Bartenstein, P.; Buerger, K.; Hiemeyer, F.; Wittemer-Rump, S. M.; Seibyl, J.; Reininger, C.; et al. Cerebral amyloid-β PET with florbetaben (¹⁸F) in patients with Alzheimer's disease and healthy controls: a multicentre phase 2 diagnostic study. *Lancet Neurol.* **2011**, *10*, 424–435.

(24) Jansen, W. J.; Ossenkoppele, R.; Knol, D. L.; Tijms, B. M.; Scheltens, P.; Verhey, F. R.; Visser, P. J.; Aalten, P.; Aarsland, D.; Alcolea, D.; et al. Prevalence of cerebral amyloid pathology in persons without dementia: a meta-analysis. *JAMA, J. Am. Med. Assoc.* **2015**, *313*, 1924–1938.

(25) Jansen, W. J.; Janssen, O.; Tijms, B. M.; Vos, S. J. B.; Ossenkoppele, R.; Visser, P. J.; Aarsland, D.; Alcolea, D.; Altomare, D.; von Arnim, C.; et al. Prevalence estimates of amyloid abnormality across the Alzheimer disease clinical spectrum. *JAMA Neurol.* **2022**, *79*, 228–243.

(26) Donohue, M. C.; Sperling, R. A.; Petersen, R.; Sun, C. K.; Weiner, M. W.; Aisen, P. S. Association between elevated brain amyloid and subsequent cognitive decline among cognitively normal persons. *JAMA, J. Am. Med. Assoc.* **2017**, *317*, 2305–2316.

(27) Sabri, O.; Sabbagh, M. N.; Seibyl, J.; Barthel, H.; Akatsu, H.; Ouchi, Y.; Senda, K.; Murayama, S.; Ishii, K.; Takao, M.; et al. Florbetaben PET imaging to detect amyloid beta plaques in Alzheimer's disease: Phase 3 study. *Alzheimer's Dementia* **2015**, *11*, 964–974.

(28) Salloway, S.; Sperling, R.; Fox, N. C.; Blennow, K.; Klunk, W.; Raskind, M.; Sabbagh, M.; Honig, L. S.; Porsteinsson, A. P.; Ferris, S.; et al. Two phase 3 trials of bapineuzumab in mild-to-moderate Alzheimer's disease. *N. Engl. J. Med.* **2014**, *370*, 322–333.

(29) Sevigny, J.; Chiao, P.; Bussière, T.; Weinreb, P. H.; Williams, L.; Maier, M.; Dunstan, R.; Salloway, S.; Chen, T.; Ling, Y.; et al. The antibody aducanumab reduces Aβ plaques in Alzheimer's disease. *Nature* **2016**, *537*, 50–56.

(30) Egan, M. F.; Kost, J.; Voss, T.; Mukai, Y.; Aisen, P. S.; Cummings, J. L.; Tariot, P. N.; Vellas, B.; van Dyck, C. H.; Boada, M.; et al. Randomized Trial of Verubecestat for prodromal Alzheimer's Disease. *N. Engl. J. Med.* **2019**, *380*, 1408–1420.

(31) Nayate, A. P.; Dubroff, J. G.; Schmitt, J. E.; Nasrallah, I.; Kishore, R.; Mankoff, D.; Pryma, D. A. Use of Standardized Uptake Value Ratios Decreases Interreader Variability of [18F] Florbetapir PET Brain Scan Interpretation. *Am. J. Neuroradiol.* **2015**, *36*, 1237–1244.

(32) Chincarini, A.; Peira, E.; Morbelli, S.; Pardini, M.; Bauckneht, M.; Arbizu, J.; Castelo-Branco, M.; Büsing, K.; de Mendonça, A.; Didic, M.; et al. Semi-quantification and grading of amyloid PET: A project of the European Alzheimer's Disease Consortium (EADC). *Neuroimage Clin.* **2019**, *23*, 101846.

(33) Peira, E.; Poggiali, D.; Pardini, M.; Barthel, H.; Sabri, O.; Morbelli, S.; Cagnin, A.; Chincarini, A.; Cecchin, D. A comparison of advanced semi-quantitative amyloid PET analysis methods. *Eur. J. Nucl. Med. Mol. Imaging* **2022**, *49*, 4097–4108.

(34) Clark, C. M.; Pontecorvo, M. J.; Beach, T. G.; Bedell, B. J.; Coleman, R. E.; Doraiswamy, P. M.; Fleisher, A. S.; Reiman, E. M.; Sabbagh, M. N.; Sadowsky, C. H.; et al. Cerebral PET with florbetapir compared with neuropathology at autopsy for detection of neuritic amyloid-β plaques: a prospective cohort study. *Lancet Neurol.* **2012**, *11*, 669–678.

(35) Joshi, A. D.; Pontecorvo, M. J.; Clark, C. M.; Carpenter, A. P.; Jennings, D. L.; Sadowsky, C. H.; Adler, L. P.; Kovnat, K. D.; Seibyl, J. P.; Arora, A.; et al. Performance characteristics of amyloid PET with florbetapir F18 in patients with alzheimer's disease and cognitively normal subjects. *J. Nucl. Med.* **2012**, *53*, 378–384.

(36) Clark, C. M.; Schneider, J. A.; Bedell, B. J.; Beach, T. G.; Bilker, W. B.; Mintun, M. A.; et al. Use of Florbetapir-PET for Imaging β-Amyloid Pathology. *JAMA, J. Am. Med. Assoc.* **2011**, *305*, 275–283.

(37) Matsuda, H.; Okita, K.; Motoi, Y.; Mizuno, T.; Ikeda, M.; Sanjo, N.; Murakami, K.; Kambe, T.; Takayama, T.; Yamada, K.; et al. Clinical impact of amyloid PET using 18F-florbetapir in patients with cognitive impairment and suspected Alzheimer's disease: a multicenter study. *Ann. Nucl. Med.* **2022**, *36*, 1039–1049.

(38) Ni, M.; Zhu, Z. H.; Gao, F.; Dai, L. B.; Lv, X. Y.; Wang, Q.; Zhu, X. X.; Xie, J. K.; Shen, Y.; Wang, S. C.; et al. Plasma Core Alzheimer's Disease Biomarkers Predict Amyloid Deposition Burden by Positron Emission Tomography in Chinese Individuals with Cognitive Decline. *ACS Chem. Neurosci.* **2023**, *14*, 170–179.

(39) Nabers, A.; Perna, L.; Lange, J.; Mons, U.; Schartner, J.; Güldenhaupt, J.; Saum, K.; Janelidze, S.; Holleczek, B.; Rujescu, D.; et al. Amyloid blood biomarker detects Alzheimer's disease. *EMBO Mol. Med.* **2018**, *10*, No. e8763.

(40) Karikari, T. K.; Pascoal, T. A.; Ashton, N. J.; Janelidze, S.; Benedet, A. L.; Rodriguez, J. L.; Chamoun, M.; Savard, M.; Kang, M. S.; Therriault, J.; et al. Blood phosphorylated tau 181 as a biomarker for Alzheimer's disease: a diagnostic performance and prediction modelling study using data from four prospective cohorts. *Lancet Neurol.* **2020**, *19* (5), 422–433.

(41) Li, Y.; Schindler, S. E.; Bollinger, J. G.; Ovod, V.; Mawuenyega, K. G.; Weiner, M. W.; Shaw, L. M.; Masters, C. L.; Fowler, C. J.; Trojanowski, J. Q.; et al. Validation of Plasma Amyloid-β 42/40 for Detecting Alzheimer Disease Amyloid Plaques. *Neurology* **2022**, *98*, e688–e699.

(42) Iaccarino, L.; Burnham, S. C.; Dell'Agnello, G.; Dowsett, S. A.; Epelbaum, S. Diagnostic Biomarkers of Amyloid and Tau Pathology in Alzheimer's Disease: An Overview of Tests for Clinical Practice in the United States and Europe. *J. Prev. Alzheimer's Dis.* **2023**, *10*, 426–442.

(43) Gordon, B. A.; Blazey, T. M.; Su, Y.; Hari-Raj, A.; Dincer, A.; Flores, S.; Christensen, J.; McDade, E.; Wang, G.; Xiong, C.; et al. Spatial patterns of neuroimaging biomarker change in individuals from families with autosomal dominant Alzheimer's disease: a longitudinal study. *Lancet Neurol.* **2018**, *17*, 241–250.

(44) Jagust, W. Imaging the evolution and pathophysiology of Alzheimer disease. *Nat. Rev. Neurosci.* **2018**, *19*, 687–700.

(45) Grimmer, T.; Shi, K.; Diehl-Schmid, J.; Natale, B.; Drzezga, A.; Förster, S.; Förstl, H.; Schwaiger, M.; Yakushev, I.; Wester, H. J.; et al. 18F-FIBT may expand PET for β-amyloid imaging in neurodegenerative diseases. *Mol. Psychiatry* **2020**, *25*, 2608–2619.

(46) McKhann, G.; Drachman, D.; Folstein, M.; Katzman, R.; Price, D.; Stadlan, E. M. Clinical diagnosis of Alzheimer's disease: report of the NINCDS-ADRDA Work Group under the Auspices of Department of Health and Human Services Task Force on Alzheimer's disease. *Neurology* **1984**, *34*, 939–944.

(47) American Psychiatric Association *Diagnostic and Statistical Manuel of Mental Disorders*; American Psychiatric Association: Washington, 1994.

(48) McKhann, G. M.; Knopman, D. S.; Chertkow, H.; Hyman, B. T.; Jack, C. R.; Kawas, C. H.; Klunk, W. E.; Koroshetz, W. J.; Manly, J. J.; Mayeux, R.; et al. The diagnosis of dementia due to Alzheimer's disease: recommendations from the National Institute on Aging-Alzheimer's Association workgroups on diagnostic guidelines for Alzheimer's disease. *Alzheimer's Dementia* **2011**, *7*, 263–269.

(49) Albert, M. S.; DeKosky, S. T.; Dickson, D.; Dubois, B.; Feldman, H. H.; Fox, N. C.; Gamst, A.; Holtzman, D. M.; Jagust, W. J.; Petersen, R. C.; et al. The diagnosis of mild cognitive impairment due to Alzheimer's disease: Recommendations from the National Institute on Aging-Alzheimer's Association workgroups on diagnostic guidelines for Alzheimer's disease. *Alzheimer's Dementia* **2011**, *7*, 270–279.

(50) Minoshima, S.; Drzezga, A. E.; Barthel, H.; Bohnen, N.; Djekidel, M.; Lewis, D. H.; Mathis, C. A.; McConathy, J.; Nordberg, A.; Sabri, O.; et al. SNMMI Procedure Standard/EANM Practice Guideline for Amyloid PET Imaging of the Brain 1.0. *J. Nucl. Med.* **2016**, *57*, 1316–1322.

(51) Xie, Q.; Ni, M.; Gao, F.; Dai, L. B.; Lv, X. Y.; Zhang, Y. F.; Shi, Q.; Zhu, X. X.; Xie, J. K.; Shen, Y.; et al. Correlation between Cerebrospinal Fluid Core Alzheimer's Disease Biomarkers and β-Amyloid PET in

Chinese Dementia Population. *ACS Chem. Neurosci.* **2022**, *13*, 1558−1565.